Phosphorus and arsenic distributions in a seasonally-stratified, iron- and manganese-rich lake: microbiological and geochemical controls

Adam Hartland[1*], Martin S. Andersen[2] and David P. Hamilton[1]

[1]Environmental Research Institute, School of Science, Faculty of Science and Engineering, University of Waikato, Hamilton, New Zealand

[2]Connected Waters Initiative Research Centre, UNSW Australia, 110 King Street, Manly Vale, NSW 2093, Australia

*Corresponding author: a.hartland@waikato.ac.nz T: +64 7 856 2889 Extn: 8527

Environmental context

Despite being present at trace concentrations (typically ppb levels), arsenic (As) and phosphorus (P) are among the most important of freshwater contaminants. This research highlights the biogeochemical coupling of P and As in a New Zealand lake. We find that the mineralisation of organic residues coupled to the dissolution of colloidal iron and manganese hydroxides may be an important driver of the bioavailability of both P and As.

Abstract

Seasonal stratification in temperate lakes greater than a few metres deep provides conditions amenable to pronounced vertical zonation of redox chemistry. Such changes are particularly evident in eutrophic systems where high phytoplankton biomass often leads to seasonally-established anoxic hypolimnia and profound changes in geochemical conditions. In this study, we investigated the behaviour of trace elements in the water column of a seasonally-stratified, eutrophic lake. Two consecutive years of data from Lake Ngapouri, North Island, New Zealand, demonstrate the occurrence of highly correlated profiles of phosphorus (P), arsenic (As), iron (Fe) and manganese (Mn), all of which increased in concentration by 1-2 orders of magnitude within the anoxic hypolimnion. Stoichiometric and mass-balance considerations demonstrate that increases in alkalinity in hypolimnetic waters were consistent with observed changes in sulfate, Fe and Mn concentrations with depth, corresponding to dissimilatory reduction of sulfate, Fe(III) and Mn(IV) hydroxides. Thermodynamic constraints on Fe, Mn and Al solubility indicate that amorphous Fe(III), Mn(IV) hydroxides most probably controlled Fe and Mn in the surface mixed layer (~0 to 8 m) while Al(III) hydroxides were supersaturated throughout the entire system. Surface complexation modelling indicated that iron hydroxides (HFO) potentially dominated As speciation in the lake, but only if other colloidal phases such as allophanic clays capable of limiting free PO_4 activity, were present. This research highlights the coupling of P, As, Fe and Mn in Lake Ngapouri, and the apparent role of multiple colloidal phases in affecting P and As activity within overarching microbiological and geochemical processes.

1. Introduction

The trace elements arsenic (As) and phosphorus (P) are among the most important of freshwater contaminants but for distinctly different reasons [1, 2]. Phosphorus is an essential, often limiting, nutrient and has a strong effect on the trophic status of water bodies where it can trigger eutrophication where present in excess [3, 4]. Arsenic is a biotoxic element which typically accumulates in iron-rich sedimentary aquifer systems [5, 6], but which is commonly present at elevated

concentrations in surface waters receiving geothermal discharges [7, 8]. Despite the quite different environmental concerns regarding P and As, their environmental fate and behaviour are often controlled by common mechanisms due to the very similar chemical structure and reactivity of their inorganic anions [9].

At circumneutral pH values, both As and P are predominantly distributed between singly and doubly charged protonated polyoxides which display similar affinities for binding with positively charged mineral surfaces. In New Zealand soils, the abundant nano-scale mineral allophane sequesters large proportions of P applied in phosphate fertilizers [10] and limits the migration of PO_4 into ground and surface waters. Consequently, sedimentary fluxes of P are a major contributor to total P loading in receiving water bodies [11]. Once present in the bottom sediments of quiescent water bodies, such as lakes, sedimentary P and As can be released by the weathering of aluminosilicates such as allophane [12-17], through cycling between organic-P and orthophosphate species [18], and by desorption from Fe and Mn hydroxide surfaces [19, 20] undergoing reductive dissolution [21]. Although the ultimate sources of P within catchments are relatively well known [11, 22], a complete picture of the processes controlling the cycling and bioavailability of P in lakes, including P speciation, remains elusive [11, 23-25], largely due to the complexity of interactions between hydrologic, geochemical and microbiological factors [25].

Lakes are particularly vulnerable to changes in the availability of nutrient elements (typically P as HPO_4^{3-} and N, as NO_3^- and NH_4^+) since increases in supply (input) may not be balanced by increases in the rate of nutrient removal (output). This is especially pertinent for P, since this element can be cycled between the water column and sediments of lakes for long periods [11], unlike N which can be removed by several mechanisms, primarily as the gas-phase species N_2O and N_2 [26, 27]. Thus, the internal recycling of P within lakes often exacerbates the problem of eutrophication [28] with associated reductions in water quality.

In warmer months, thermal stratification of lakes limits vertical mixing, and therefore prevents equilibration of deeper (hypolimnetic) waters via atmospheric gaseous exchange. By definition, warm monomictic lakes only completely mix once per year, meaning that for long periods, typically from to spring to autumn, they are subject to thermally induced stratification [29]. This well-known process limits the diffusion of dissolved oxygen from the atmosphere to the deeper hypolimnetic waters, leading to the seasonal establishment of hypolimnetic anoxia in lakes with an abundant supply of organic matter to this zone [26]. The aforementioned anoxic conditions thus lead to a sequential titration of oxidant species present from the time the lake was fully mixed. These oxidant species act as terminal electron acceptors in the microbiological degradation of natural organic matter.

This study targeted a monomictic lake known to display increases in NH_4^+, Fe and Mn following stratification [30]. We set out to produce a highly resolved picture of the vertical redox zonation within the lake profile in order to better understand the controls on the biogeochemical cycling of nutrients (C, N and P) and other trace elements within this system.

2. Methods and Materials

2.1 Study site

Lake Ngapouri (Supplementary Figure 1), is a small (0.19 km^2) monomictic, eutrophic lake within a hydrothermal explosion crater formed during the Kaharoa eruption of 636 ± 12 calendar yr BP [31].

The lake has a maximum depth of 24.5 m and is thermally-stratified for nine months of the year [32]. During seasonally-established hypolimnetic anoxia in the lake, increases in the concentrations of Fe, Mn and NH_4^+, and decreases in SO_4^{2-} occur in Ngapouri sedimentary pore waters [30]. It has also been noted that the polyoxides (P and As) and chalcophilic elements (Cu, Zn, Pb, Hg) are also affected by redox cycling to some extent, possibly in association with Fe, Mn and S [30].

2.2 Sampling

Sampling campaigns at Lake Ngapouri were completed during the late summer of 2013 and 2014 coinciding with the first weekend of March. Two highly resolved vertical profiles of the entire water column were obtained using a Schindler-Patalas trap ato collect water at 0.5 m intervals between depths of 0 and ~23 m, thus capturing the entire epilimnion, hypolimnion and top of the benthic nepheloid layer (water within ~0.5 m of the sediment surface). Samples of 100 mL lake water were collected in pre-cleaned HDPE bottles (dilute HNO_3 and deionised water wash) after being rinsed three times with the sample water prior to collection. Care was also taken to leave no head space in the bottles which were then sealed with tape as an additional measure. The samples were then kept in the dark and chilled at < 5°C. Because we did not seek to determine gaseous species, no additional attempt was made to limit degassing of H_2S, which was clearly present in hypolimnetic samples based on its pungent odour. Indeed, degassing of H_2S during filtration and storage of the samples prior anion analysis was considered to be preferable so as to limit the potential for re-oxidation to sulfate. Comprehensive physiochemical profiles of the Ngapouri water column were produced using a conductivity-temperature-depth (CTD) profiler (Sea Bird Electronics, 19 plus SEACAT Profiler), fitted with dissolved oxygen (DO, detection limit of 0.1 mg L^{-1}), conductivity, temperature and chlorophyll fluorescence probes (Seabird Electronics, Bellvue, WA). Four profiles were completed with the CTD probe in each year, in order to provide a comprehensive spatial coverage of the physiochemical variability of the water column.

2.3 Analytical methods

Upon return to the laboratory, samples were filtered under vacuum through 0.45 μm Whatman GF/F filters using HNO_3/deionised-water-washed Büchner funnels and flasks. In this procedure, filters were first washed using dilute HNO_3 and deionised water following the procedure described elsewhere [33], allowed to dry, and then used to filter the samples. Individual aliquots were collected for trace elements, anions and bicarbonate alkalinity. The filtration step was sufficiently rapid (< 10 s) to avoid oxidative-loss of reduced Fe(II) and Mn(II) on the filter membrane, since the samples had remained sealed since collection. However, it should be noted that the speciation of redox sensitive species were not determined analytically in this study and therefore we present the total concentrations of trace elements only.

The filter membrane used in this study was sufficiently coarse (~0.45 μm) that any freshly-precipitated iron and manganese colloids (with probable dimensions in the nanometre range) were unlikely to be retained by the filters. Trace element samples were immediately acidified following filtration with 2% by volume analytical grade HNO_3 and analysed on a Perkin Elmer (Waltham MA) quadrupole ICPMS calibrated with NIST-traceable standards (Inorganic ventures, Christiansburg, VA). Five procedural blanks using deionised water (18 mΩ) returned values for most trace elements that were below detection limits (typically < 1 ppb). The mean concentrations of Na, Mg, Si, K, Ca, Fe and Zn in the procedural blanks were 9 ± 8 ppb, 1 ± 1 ppb, 2 ± 9 ppb, 1 ± 1 ppb, 2 ± 3 ppb, 26 ± 19, 1 ± 1 ppb, and 2 ± 2 ppb, respectively. All reported concentrations for the aforementioned elements

were blank-corrected to mean value. The analytical uncertainty for all elements reported by ICPMS is therefore much smaller than the associated sampling uncertainty and is not considered further.

A full suite of inorganic anions was also determined for all samples collected in 2014 using a Dionex Ion Chromatography system equipped with a Dionex IonPac AS18-4µm Hydroxide-Selective Anion-Exchange Column (Thermo Scientific, Waltham MA). Standards and samples were run using a 25 mM NaOH isocratic method with electrolytic ion suppression at an operating pressure of ~2700 psi. Nutrient species were also determined by flow injection analysis (FIA) (NO_x, NO_2^-, NO_3^-, NH_4^+, PO_4^{3-}) using standard methods [34] which yielded limits of quantification of 0.004, 0.002 and 0.001 mg L^{-1} for PO_4-P, NH_4-N and NO_3-N/NO_2-N, respectively. Bicarbonate alkalinity was measured using a Metler-Toledo (Columbus, OH) auto-titrator system, using 0.1 M HCl and titrated against pH to the CO_2 equivalence point. Alkalinity was then quantified using the Gran method.

Overall, the inorganic geochemical dataset produced in 2014 was of good quality, although the pH values for profile 2 are considered to be less reliable, given their noisier distribution with depth. In Tables 1 and 2, the ion balance data from profiles 1 and 2 are provided. The charge balance error associated with the chemical analyses was calculated in PHREEQC version 2.17.01 [35]. The charge balance error analysis from profile 1 was typically less than 3% (average = -2.44%, 1σ= 3.31%). For profile 2, the charge balance error was typically less than 2% (average = -1.68%, 1σ= 4.15%).

2.4 Geochemical modelling

Inorganic equilibrium modelling of lake water samples was completed using PHREEQC version 2.17.01 [35] to calculate the saturation indices of mineral phases and oxidation states of redox sensitive elements. In addition, the geochemical model Visual MINTEQ 3.0 was used to simulate surface complexation reactions between hydrous ferric oxide (HFO)[36], $5Fe_2O_3 \bullet 9H_2O$, hydrous manganese oxide (HMO), MnO_2[37], and gibbsite-DLM, $Al(OH)_3$[38]. These solids have default specific surface areas of 600, 746 and 32 (m^2 g^{-1}), respectively. The complexation databases employed were feo-dim_2008.cdb, hmo-dim_tonkin.cdb, gt_std.cdb. Modelling was carried out using a spherical geometry and geometric radii of 1 nm and with counter ion accumulation enabled. The concentrations of the dispersed surface phases was calculated using the average concentrations of Fe, Mn and Al in the surface mixed layer of Lake Ngapouri, assuming the relevant pure-phase stoichiometry.

3. Results

Physiochemical gradients in Lake Ngapouri (2013-2014)

Physiochemical depth profiles of Lake Ngapouri from March 2013 and 2014 demonstrate that thermal stratification (Figure 1a) and an anoxic hypolimnion (Figure 1b) were established in the lake in both years. The density discontinuity occurred at ~6m in 2013 and ~8m in 2014. In both years, phytoplankton chlorophyll *a* (indicated by a proxy of chlorophyll fluorescence from the CTD probe) was centred on this density discontinuity (epilimnion-hypolimnion interface) (Figure 1e). Profiles of specific conductance (Figure 1b) reveal several distinct regions of geochemical interest within the lake profile:

(i) Epilimnion: stable conductance values, indicating a well mixed condition
(ii) Epilimnon-hypolimnion interface: a marked depletion in conductance

(iii) Anoxic hypolimnion to ~5m from the lake bottom: a monotonic increase in dissolved ions with depth

(iv) Bottom waters to benthic nepheloid layer: a slower increase in conductance towards the sediment-water interface.

Overall, the physiochemical data indicate that large changes in lake water chemistry occurred beneath the thermocline in both years. In 2014 a comprehensive geochemical dataset was acquired permitting the dominant geochemical reactions driving changes in EC to be examined.

pH data from Ngapouri in 2013 were concordant with the measured changes in the other variables (Figure 1c). However, in 2014 a faulty pH probe prevented the acquisition of high resolution pH data. The data from 2014 that are presented in Figure 2c were measured using a benchtop pH meter in the laboratory.

Biogeochemical controls on major ion chemistry (2014 data)

The major ion dataset from the March 2014 sampling is shown in Figure 2. Overall, the largest changes in major ion concentration centred on sulfate and bicarbonate, indicating a prominent redox control beneath the thermocline at ~8 m. Nitrate was undetectable using ion chromatography (LD 0.1 mg L^{-1}) in 2014 and was also below detection limits in 2013 when analysed using the more sensitive technique of flow injection analysis [(FIA), LD 0.05 mg L^{-1}]. The FIA data from 2014 do indicate very low levels of nitrate were present in the epilimnion from profile 2 (Table 2). However, the remaining nitrate and nitrite data are very low level and when detected probably reflect some very small degree of oxidation of reduced N species following collection. Given the absence of nitrate in hypolimnetic waters, the large changes in sulfate and bicarbonate appear to be consistent with the loss of sulfate by reduction to hydrogen sulfide by sulfate-reducing bacteria involved in the respiration of organic carbon (here simplified to CH_2O), according to the overall equation:

$$SO_4^{2-} + 2CH_2O \rightarrow H_2S + 2HCO_3^- \quad (1)$$

This process consumes two moles of acidity for every mole of sulfate reduced. Thus, if the loss of sulfate with depth is the result of sulfate reduction, then the observed changes in alkalinity can be directly related to changes in sulfate concentration because alkalinity is related to mineral acidity (H-Acy) by the relation:

$$\text{H-Acy} = [H^+] - [HCO_3^-] - 2[CO_3^{2-}] - [OH^-] \quad (2)$$

Therefore, alkalinity corresponds to the negative of H-Acy.

$$\text{Alk} = -\text{H-Acy} \quad (3)$$

In Figure 3a-b, the change in sulfate and bicarbonate (HCO_3^-) alkalinity in profiles 1 and 2 from 2014 are shown following normalisation to the Cl^- concentration at the same depth. Since Cl^- can be considered to be conservative under the low ionic strength conditions in Lake Ngapouri, normalising to Cl^- provides a means of determining the change in SO_4^{2-} and HCO_3^- species that is not attributable to variations in the source water. Interestingly, this approach indicates that the large change in sulfate between 8 and 22 m was driven by sulfate removal within the water column, rather than hydrodynamic factors. This approach to the analysis of sulfate and alkalinity data is supported by previous monitoring of Lake Ngapouri surface and benthic waters between November 2007 and

November 2008. This monitoring demonstrated that the total S concentration in the surface waters was very stable throughout the year, averaging 7.30 ± 1.13 ppm over the course of the year [30]. When compared to the average epilimnetic total S concentrations measured in 2013 and 2014 of 7.40 ± 0.5 ppm and 7.40 ± 0.2 ppm, this indicates a high degree of stability in the epilimnetic S budget. Assuming that bacterial sulfate reduction was the driver of the observed change in sulfate, we can calculate the change in bicarbonate alkalinity (ΔHCO_3) expected for the corresponding loss of sulfate.

The predicted change in alkalinity (ΔHCO_3) was calculated from the observed change in sulfate concentration (ΔSO_4) at each depth, relative to the average sulfate concentration in the upper ten metres of the lake for each profile (i.e. with respect to (wrt) 0 – 10 m), using the relation:

$$\Delta x = \frac{[x]_n}{[x]_{0\text{-}10}} \quad (4)$$

where Δx is the change in a species x at depth n relative to the upper oxidised and mixed layer (0-10 m). This calculation used a SO_4:HCO_3 ratio of 1:2.

Because the epilimnion was well mixed and able to approach equilibrium with atmospheric O_2, no change in sulfate would be expected within this layer. Indeed, only a small degree of variance in SO_4 and HCO_3 was observed. Thus, this approach is reasonable from both hydrodynamic and geochemical perspectives.

It is clear from Figure 3 (c-d) that the consumption of acidity by sulfate reduction was insufficient to explain the total change in alkalinity. Indeed, sulfate reduction consistently under-predicted ΔHCO_3 in both profiles of the lake (Fig. 5a). The estimated change in alkalinity due to sulfate reduction left a residual average proportion of 32.7 to 40.7% ΔHCO_3 (profile 1 and 2, respectively) unaccounted for in the hypolimnion. Therefore secondary, geochemically-plausible mechanisms are required to account for this discrepancy.

In addition to the pronounced changes in sulfate and alkalinity observed in the 2014 dataset, large variations in the total concentration of Fe and Mn were also observed (Fig. 4b and 4c) with both Fe and Mn increasing in concentration with the anoxic hypolimnion, consistent with previous measurements of Fe and Mn in epilimnetic and hypolimnetic waters [30]. Between the epilimnion and hypolimnion, Fe ranged from ~0.04 to ~4 mg L^{-1}, and Mn from 0.02 to 0.7 mg L^{-1}. Whilst acknowledging the complexity of the processes driving Fe and Mn dynamics in lake systems [19, 20, 39, 40], we sought, as a first approximation, to determine how much of the observed change in ΔHCO_3 could be accounted for by within-lake dissimilatory Fe(III) and Mn(IV) reduction via the overall reactions:

$$CH_2O + 4Fe(OH)_3 + 7H^+ \rightarrow 4Fe^{2+} + HCO_3^- + 10H_2O \quad (5)$$

$$CH_2O + 2MnO_2 + 3H^+ \rightarrow 2Mn^{2+} + HCO_3^- + 2H_2O \quad (6)$$

Note that equations 5 and 6 both produce Mn(II)/Fe(II) and alkalinity in equimolar amounts. We assumed that iron was most likely to be present in the form of freshly-formed amorphous hydroxides.

In profile 1 (Figure 4b), the observed change in Fe(total) between the upper oxidised layer and the benthic nepheloid layer was 2.23 times greater than measured in profile 2 (Figure 4c). By comparison, the observed change in Mn(total) between the upper oxidised layer and the bottom waters of both profiles was virtually identical. Taking the ratio of $\Delta Fe_{surf\text{-}bottom}/\Delta Mn_{surf\text{-}bottom}$ gives values of 5.84 and 2.76 for profiles 1 and 2, respectively. Assuming that the contribution of reactions 5 and 6 to ΔHCO_{3obs}-ΔHCO_{3pred} follows this ratio, the change in Fe(II) and Mn(II) can be predicted from equations 5 and 6. This also assumes that Mn and Fe reduction accounted for all of the residual ΔHCO_3 in the lake profiles not explained by ΔSO_4 and that the Fe-oxyhydroxides were present in more soluble forms (less stabile forms: amorphous to Goethite) in order to be reduced entirely before onset of sulfate reduction [41].

In deriving the predicted change in Mn(II) and Fe(II) shown in Figure 4b and c, we assumed that dissimilatory iron reduction was insignificant in upper oxidised layer and therefore we only plot the data where the values become consistently positive. Since, if ΔFe is negative then ΔHCO_{3obs}-ΔHCO_{3pred} is also negative and therefore meaningless. With respect to Mn, the plots in Fig. 4b-c demonstrate that the estimated increase in Mn(II) due to dissimilatory manganese reduction closely corresponded to the increase in total Mn between depths of 8 and 12 m in profile 1 and 5-10 m in profile 2. Below these points, total Mn increased relative to the estimated increase in Mn(II). This disparity was relatively minor in profile 1, corresponding to a mean difference of 25.0 ± 20.6% (1σ), compared to a mean difference of 85.7± 8.0% (1σ) in profile 2. This suggests that in profile 2 a large proportion of Mn total was not supported by bacterial reduction of manganese oxides in the water column but instead represents a more significant sedimentary Mn(II) flux originating from the Benthic nepheloid layer [26].

In contrast to Mn, the estimated increase in Fe(II) due to dissimilatory iron reduction over-predicted the initial increase in Fe total in the upper first few metres of the anoxic hypolimnion. However, in both profile 1 and 2, total Fe concentrations showed marked reductions within this region [corresponding to the density discontinuity and deep chlorophyll maximum (DCM)]. Following this point, at depths of around 12 to 15 m Fe total concentrations showed improved agreement with predicted increases in Fe(II). The mean difference between the observed ΔFe totals and predicted $\Delta Fe(II)$ was -7.7 ± 38.5% below 12m in profile 1, and -16.4 ± 42.5% below 12m in profile 2.

Overall this analysis of the HCO_3 mass balance in Ngapouri and the estimated contributions of Fe(III), Mn(IV) and sulfate reduction to ΔHCO_3 indicate that sulfate reduction is dominant in mass terms and that the reduction of Fe and Mn oxides within the hypolimnion is likely to play an important role in major and trace element distributions. Since it is known that the entire water column is uniform with respect to Fe and Mn during the mixed period at ~0.5 and ~0.2 mg L^{-1} respectively (June to early September) [30], and that during the onset of stratification and oxygen depletion in the hypolimnion, both Fe and Mn increase in concentration, and the decline again. Therefore, this implies that

i) additional Mn(II) and Fe(II) is added to the system (from the benthic nepheloid layer)
ii) further removal mechanisms begin to act on total Fe and Mn concentrations during the stratified period

One process that accounts for all of these changes is the precipitation of Fe(III) and Mn(IV) hydroxides in the epilimnion fuelled by a large diffusive concentration gradient from the benthic nepheloid layer [30]. This therefore reinforces the findings of previous workers which point to the

284 important roles played by exchange with the sediment, and the positional time dependence of sinking
285 particles and diffusing colloids which may be reductively dissolved [19, 40].

286

287 *Geochemical speciation modelling of Lake Ngapouri*

288 To test the extent to which the hypothesised role of Fe(III) and Mn(IV) hydroxides was physically
289 realistic, geochemical speciation modelling of the entire water column of the lake (profiles 1 and 2)
290 were carried out using the PHREEQC computer program and standard database (phreeqc.dat).
291 Saturation index (SI) values of various mineral phases were calculated at each depth, with pe values
292 calculated using the O(-2)/O(0) redox couple in the epilimnion and the SO_4/H_2S redox couple in the
293 hypolimnion. Concentrations of H_2S were estimated by assuming that H_2S increased and SO_4
294 decreased in equimolar amounts according to Equation 1. This estimate was again made with respect
295 to the average SO_4 concentration in the upper 10 m and assumed that the H_2S concentration in the
296 oxidised epilimnion was zero. This approach had the additional benefit of allowing the saturation
297 indices (SI) of sulfide minerals to be estimated.

298 Modelling of SI values for pure mineral phases in equilibrium with Lake Ngapouri waters
299 demonstrated that the entire water column was subsaturated with respect to the carbonate minerals
300 calcite ($CaCO_3$), rhodochrosite ($MnCO_3$) and siderite ($FeCO_3$), although siderite comes close to
301 saturation towards the bottom of the lake. SI values for silica-oxides increase over depth with
302 supersaturation indicated for quartz (SiO_2), but subsaturation for more soluble amorphous silica
303 oxides [SiO_2(a)]. It is likely that a silica-oxide of intermediate solubility is controlling the dissolved
304 silica content in the hypolimnetic waters.

305 Supersaturation was observed in the oxidised epilimnion, with respect to several important mineral.
306 Namely, amorphous iron hydroxide $Fe(OH)_3$(a), goethite (FeOOH), pyrolusite (MnO_2), and for the
307 entire water column with respect to imogolite [$(HO)_3Al_2O_3SiOH$] and gibbsite [$Al(OH)_3$] (Figure 5a-
308 d). Saturation indices for the Al-bearing phases, including halloysite and boehmite, suggest that Al
309 solubility was probably controlled by an AlOH phase, such as paracrystalline imogolite or the more
310 amorphous allophane. Predictable changes were also seen in redox-sensitive arsenic, for which As(V)
311 dominated in the surface mixed layer and the more toxic As(III) was most prevalent in the anoxic
312 hypolimnetic waters. This modelling also predicted some precipitation of iron mono-sulfides and
313 mackinawite with SI values > 1 at depth, as would be expected (Figure 5e-f).

314 Overall, this exercise demonstrates that thermodynamic constraints on the solubility of Fe and Mn
315 under oxidising conditions in the epilimnion are likely to drive the formation of insoluble Fe(III) and
316 Mn(IV) oxides in Lake Ngapouri during the stratified period. It is reasonable to predict that this
317 process would be further fuelled by the diffusion of Fe(II) and Mn(II) from the anoxic hypolimnion
318 and that diffusion of $Fe(OH)_{3(a)}$ and MnO_2 colloids into the hypolimnion would also occur.
319 Subsequent reductive dissolution of these oxides (with release of adsorbed ions) in the hypolimnion
320 could re-release Fe(II) and Mn(II) to maintain the upward diffusive flux and cycle these trace
321 elements through the boundary layer many times over.

322 Oxides of aluminium were supersaturated throughout the water column with the highest values
323 reported for imogolite. Imogolite may be more thermodynamically stable than gibbsite since it has
324 slower dissolution kinetics [42, 43]. This is probably significant for the behaviour of multiply charged
325 anions within the lake, since aluminium hydroxides such as imogolite have very high anion adsorption
326 capacities [13, 15, 16].

Overprint of redox zonation on trace element distributions

In addition to major ion chemistry, a suite of 28 trace elements was determined using ICPMS. This produced a large dataset [n=55 (2013), n=90 (2014)]. Most prominent in this dataset was the overprint of redox zonation on trace element abundances. Several elements displayed clear enrichments within the hypolimnion and strong Pearson cross correlation coefficients (Supplementary Table 1). In order to determine the extent to which variations in trace elements were affected by redox processes in Lake Ngapouri, principle component analysis (PCA) of the entire 2014 dataset was undertaken (Figure 6).

In Figure 6, the impact of redox zonation can be clearly seen in the separation of trace elements by the first two principal components which explain 60.6% of the variance in the dataset. Principal component 1 most clearly separates Cr, Ni, Hg, Sb, Au, Cu and Tl from Na, Si, Co, Zn, Mn, Fe, P, As and U. Simple elemental classification schemes cannot explain the full extent of variance seen here, although the first group appears to be distinguished on the basis of its insolubility in the presence of sulfides (chalcophiles), particularly Au and Hg. However, the second group includes elements with a range of affinities for combining with oxygen (lithophiles), sulphur and iron (siderophiles).

We suggest that the second group of elements therefore consists of elements released from the lake sediments during the establishment of the anoxic hypolimnion and which is mobilised as a result of the diagenesis of sedimentary organic matter (P), primary [sodium feldspars (Na, Si, Al)] and secondary [iron, aluminium and manganese hydroxides (Fe, Mn, Al)] mineral phases. Based on this interpretation, the very strong association between Fe and As (R^2=0.99) stands out as an anomaly (Figure 7). Yet, this elemental pairing shows the strongest correlation in both the 2013 and 2014 datasets.

Arsenic is known to have a strong association with Fe hydroxides and in particular, is known to increase in concentration in groundwaters as a result of the reductive dissolution of Fe(III) hydroxides in sedimentary aquifers [44]. The tight coupling of As and Fe within this system is consistent with both a sedimentary source originating from the benthic nepheloid layer, but also a strong association within the water column as a whole. We therefore suggest that the only plausible mechanism which can account for this strong association of iron and arsenic under both oxidising and reducing conditions is the surface complexation of As(V) by Fe(III) hydroxides and their subsequent reductive dissolution leading to the ultimate release of As(III) under reducing conditions. At the circumneutral pH of Lake Ngapouri, we would predict that As(III) distributions would also be impacted by sorption reactions with Fe(III) hydroxide surfaces which persist to some extent in the hypolimnion [45].

In addition to Fe and As, the trace elements P, Mn and Si were highly correlated in the profiles of Lake Ngapouri from both March 2013 and 2014. Given the similar affinity of P (as PO_4^{3-}/HPO_4^{2-}/$H_2PO_4^-$) and As (AsO_4^{3-}/$HAsO_4^{2-}$/$H_2AsO_4^-$) for binding with Fe and Mn hydroxides [46-48] and aluminosilicates [15, 16], the possibility that that all four elements were controlled by a combination of surface complexation and reductive dissolution requires investigation.

In Figure 7a, the tight correlation of dissolved (< 0.45 μm) Fe and As in both years is shown. Dissolved arsenic and phosphorus profiles in Lake Ngapouri (Figure 7b-c) showed the clear overprint of redox zonation with both elements increasing significantly within the anoxic hypolimnion (delimited by the DO_2 concentration). In profile 1 from 2014, a particularly strong increase in P [and PO_4^{3-} (Figure 2)] was observed which was centred on the thermocline and coincided spatially with the deep chlorophyll maximum. Interestingly, in 2014 both the DCM and P peaks in profile 1 were larger

than in profile 2, indicating a higher level of biological activity in the more P-rich waters and a possible second-order control on the establishment of the DCM [29].

Surface complexation modelling of As, P and trace metals with Fe, Mn and Al hydroxides

Both P and As are known to have a strong affinity for binding with positively charged mineral surfaces in natural waters [48]. The process of arsenate (AsO_4^{3-}) and phosphate (PO_4^{3-}) adsorption to Goethite has been shown to have a 1:1 stoichiometry [48], and hence proportions of arsenate and phosphate adsorbed at iron oxide surface sites is a function of their respective concentrations, the concentration of other competing ions, the surface area and binding site density of the respective oxides. Where Fe, Mn and Al oxides are dispersed as nanoparticles and colloids [49] both arsenic and phosphorus may therefore be adsorbed to their surfaces. This is also a pH-dependent process, due to the effect of pH on surface charge. Hence, variations in ambient pH will affect the applicability of any modelling results. Furthermore, environmental colloids are likely to have divergent surface area and charge characteristics from those used in models due to a number of processes including charge heterogeneity, organic surface films and aggregation [49]. Nevertheless, a modelling approach can be highly informative if these factors are taken into account.

Surface complexation modelling of P, As and trace metal adsorption to hydrous ferric oxide (HFO; 0.2 mg L^{-1}), hydrous manganese oxide (HMO; 0.01 mg L^{-1}) and gibbsite [$Al(OH)_2$; 0.04 mg L^{-1}], was carried out using the geochemical model VMINTEQ 3.0 at the average geochemical conditions in the upper ten metres of Lake Ngapouri in March 2014. Initially, the modelled adsorption of P and As assumed that total P and As measured by ICPMS was representative of the ambient phosphate and arsenate concentrations. However, this returned results which indicated that only around 10% of total P and As was likely to present in surface complexes.

A cross-comparison of the ICPMS and FIA data (Figure 8) demonstrates that the ICPMS data was generally a very good predictor of phosphate concentration determined by FIA, except at the low total P concentrations of the epilimnion and hypolimnion. In the epilimnion the ICPMS-supported phosphate concentration was ~0.04 mg L^{-1} compared to phosphate by FIA being < 0.01 (limit of quantification). The origin of this discrepancy is most likely due to other forms of P such as organic-P species that are not hydrolysed to phosphate in the acidic FIA mixture, but which appear in the ICPMS signal. In the hypolimnion, the ICPMS data also over predicted the concentration of phosphate leading to the observed departure from the 1:1 slope at lower concentrations in Figure 8. Model results using phosphate concentrations of 0.01 mg L^{-1} and arsenate concentrations of 0.003 mg L^{-1} indicated that of the three mineral phases, HFO was likely to be the most important with respect to both P and As (up to ~29% total As, and ~42% total P surface adsorbed) (Figure 9). However, the estimate of As adsorption by the model was inconsistent with the highly significant correlations between Fe and As observed in both years (R^2=0.99), which indicate a direct and highly consistent chemical mechanism controlling As and Fe in this system.

In order to test the hypothesis that As could have been controlled by Fe hydroxides, modelling of arsenate complexation by HFO was carried out in the absence of phosphate. This confirmed that HFO had the potential to dominate the speciation of As (~98% As in the form of AsO_4 surface-adsorbed) in this system. This indicates that arsenic (as arsenate in oxygenated surface waters) may have been mainly complexed by colloidal iron hydroxide surfaces, but only if another carrier phase such as a colloidal aluminosilicates mineral [12] was able to complex phosphate, and thereby reduce the activity of phosphate ions competing for surface sites on amorphous iron hydroxides.

We can speculate therefore that increases in As in the anoxic hypolimnion probably correspond to the release of As following the reductive dissolution of Fe oxides. Simultaneous to this As release, phosphate was released in very high concentrations (Figure 2). It is likely that the increases in phosphate probably relate to P release from decaying phytoplankton, rather than due to the dissolution of any mineral phases (Figure 2 and 7).

A major discrepancy in this modelling exercise is the exclusion of aluminosilicates with higher capacities for anion adsorption for which surface complexation models aren't readily available. Our equilibrium speciation calculations in PHREEQC suggest that imogolite was oversaturated throughout the entire water column. Thus, it is probable, given the high specific surface areas (~150-580 m^2 g^{-1}) and high anion adsorption capacities of imogolite and allophane [13], that a small amount of these minerals could account for the aforementioned discrepancy in As complexation.

4. Discussion

In stratified monomictic lakes, like Ngapouri, trace elements become redistributed throughout the water column during vertical mixing in the autumn and winter. This has clear ramifications for the bioavailability of both nutrient and toxic elements during these periods. For example, in our modelling As(III) was predicted to dominate As speciation in hypolimnic waters. However, during periods of mixing, this toxic As(III) will be redistributed within the water column and ultimately oxidised back to As(V) as the waters approach equilibrium with the atmosphere. One question that arises therefore, is at what rate does this re-oxidation occur and to what extent is this recycled As(III)/As(V) adsorbed to newly precipitated Fe hydroxide surfaces and existing Al/Si hydroxides like allophane?

Evidence from the only previous geochemical study of Lake Ngapouri [30] indicates that Fe and Mn decline in concentration prior to and following mixing. This indicates that the formation of insoluble Fe(III) and Mn(IV) hydroxides and possibly sulfides throughout the water column is followed by their destabilisation and sedimentation. On the basis of the modelling presented here, we may speculate that much of the dissolved As(III)/As(V) becomes re-adsorbed to these newly-precipitated hydroxides and is also temporarily sequestered to the bottom sediments.

Complexation reactions between iron hydroxide surfaces [48], Al/Si hydroxides [12, 15-17], and competing anions are likely to have an important bearing on the bioavailable pool of dissolved arsenic and phosphorus in New Zealand's lake systems in the North Island. The pH-sensitivity of these reactions is another important consideration which may play an essential role in modulating bioavailable P and As concentrations on a range of temporal scales. At pH values of 8 and above, most iron hydroxides attain negative surface charge characteristics [50], and hence are predicted to no longer play a significant role in As or P speciation. This implies that under high pH conditions, as commonly occurs in surface waters of many eutrophic lakes which are characterised by strong biological demand for inorganic carbon, P and As involved in complexation reactions with Fe hydroxides may become more bioavailable with potential implications for freshwater quality and eutrophication. Conversely, both imogolite and allophane both have isoelectric (pH_0) points close to pH 10 or even higher [51]. This means that anions like phosphate and arsenate may be electrostatically adsorbed or specifically complexed by these mineral phases even at the very high pH conditions characteristic of eutrophic lakes.

Our results reinforce a previous study [29] which found strong peaks in the vertical distribution of chlorophyll [Deep Chlorophyll Maximum; DCM)] in close association with the thermocline of

stratified Rotorua lakes. The earlier study had limited vertical resolution of nutrient concentrations, however, and hypothesised that the DCM was supported by a balance of sufficient light for net photosynthetic activity (> 1% of surface light values) with upward diffusion of growth-promoting nutrients sourced from regeneration in the hypolimnion. Our results suggest a more complicated distribution of phosphate with peaks immediately above and below (within 1-2 m) the DCM. Vertical profiles of specific conductance point to a relatively well-mixed surface layer (uniform conductivity), a discontinuity at the thermocline where there is low-conductivity water and a weakly mixed hypolimnion where conductivity increases almost linearly with depth. The latter points to a diffusional gradient of dissolved ions associated with benthic sediment-mediated releases. By contrast, the discontinuity at the thermocline suggests an external source of water, possibly nutrient-rich inflows that help to support the DCM. Alternatively, this discontinuity may represent the depletion of dissolved ions due to high biological demand associated with the DCM. Clearly, further high-resolution vertical sampling as part of a time series is needed to better understand the dynamics of the DCM, its second order effects on vertical distributions of anions and cations, and the species of phytoplankton that constitute it.

5. Conclusion

The results of this study point to the role of colloidal iron hydroxides in controlling the cycling of arsenic in iron-rich lake systems. Strong correlations between elemental abundances may be consistent with linked geochemical and microbiological controls over P, As, Fe and Mn in Lake Ngapouri. Our analysis indicates that there driving mechanisms that lead to this correlation may involve multiple colloidal phases, strong redox gradients and the high biological turnover of orthophosphate. Further work is needed to understand how variations in the availability of iron, manganese and Al/Si hydroxide surfaces may control the bioavailability of As and P in New Zealand's lake systems, and to what extent these processes are modulated by fluctuations in redox chemistry and pH.

6. Acknowledgements

This study was funded through the University of Waikato Lakes Chair supported by Bay of Plenty Regional Council. We are grateful to University of Waikato staff members Ronald Ram (FIA), Annie Barker (fieldwork) and Steve Cameron (ICPMS) for their technical assistance in the completion of this research.

7. References

[1] Frisbie SH, Ortega R, Maynard DM, Sarkar B. The concentrations of arsenic and other toxic elements in Bangladesh's drinking water. Environmental Health Perspectives. **2002**, 110(11), 1147-53.
[2] Paerl HW, Hall NS, Calandrino ES. Controlling harmful cyanobacterial blooms in a world experiencing anthropogenic and climatic-induced change. Science of the Total Environment. **2011**, 409(10), 1739-45.
[3] Lewis Jr WM, Wurtsbaugh WA. Control of lacustrine phytoplankton by nutrients: Erosion of the phosphorus paradigm. International Review of Hydrobiology. **2008**, 93(4-5), 446-65.
[4] Lewis WM, Wurtsbaugh WA, Paerl HW. Rationale for control of anthropogenic nitrogen and phosphorus to reduce eutrophication of inland waters. Environmental Science and Technology. **2011**, 45(24), 10300-5.

[5] Postma D, Larsen F, Thai NT, Trang PTK, Jakobsen R, Nhan PQ, et al. Groundwater arsenic concentrations in Vietnam controlled by sediment age. Nature Geoscience. **2012**, 5(9), 656-61.
[6] Nordstrom DK. Worldwide occurrences of arsenic in ground water. Science. **2002**, 296(5576).
[7] Lord G, Kim N, Ward NI. Arsenic speciation of geothermal waters in New Zealand. Journal of Environmental Monitoring. **2012**, 14(12), 3192-201.
[8] Robinson B, Outred H, Brooks R, Kirkman J. The distribution and fate of arsenic in the Waikato River system, North Island, New Zealand. Chemical Speciation and Bioavailability. **1995**, 7(3), 89-96.
[9] Linge KL, Oldham CE. Control mechanisms for dissolved phosphorus and arsenic in a shallow lake. Applied Geochemistry. **2004**, 19(9), 1377-89.
[10] Rivaie AA, Loganathan P, Graham JD, Tillman RW, Payn TW. Effect of phosphate rock and triple superphosphate on soil phosphorus fractions and their plant-availability and downward movement in two volcanic ash soils under Pinus radiata plantations in New Zealand. Nutrient Cycling in Agroecosystems. **2008**, 82(1), 75-88.
[11] Hickey CW, Gibbs MM. Lake sediment phosphorus release management-Decision support and risk assessment framework. New Zealand Journal of Marine and Freshwater Research. **2009**, 43(3), 819-56.
[12] Fish GR. Lake Rerewhakaaitu - an apparently phosphate - free lake. New Zealand Journal of Marine and Freshwater Research. **1978**, 12(3), 257-63.
[13] Gustafsson JP. Modelling competitive anion adsorption on oxide minerals and an allophane-containing soil. European Journal of Soil Science. **2001**, 52(4), 639-53.
[14] Su C, Harsh JB. Dissolution of allophane as a thermodynamically unstable solid in the presence of boehmite at elevated temperatures and equilibrium vapor pressures. Soil Science. **1998**, 163(4), 299-312.
[15] Arai Y, Sparks DL, Davis JA. Arsenate adsorption mechanisms at the allophane - Water interface. Environmental Science and Technology. **2005**, 39(8), 2537-44.
[16] Parfitt RL. Phosphate reactions with natural allophane, ferrihydrite and goethite. Journal of Soil Science. **1989**, 40(2), 359-69.
[17] Parfitt RL. Allophane in New Zealand - a review. Australian Journal of Soil Research. **1990**, 28(3), 343-60.
[18] Özkundakci D, Hamilton DP, McDowell R, Hill S. Phosphorus dynamics in sediments of a eutrophic lake derived from 31P nuclear magnetic resonance spectroscopy. Marine and Freshwater Research. **2014**, 65(1), 70-80.
[19] Davison W. Iron and manganese in lakes. Earth-Science Reviews. **1993**, 34(2), 119-63.
[20] Hamilton-Taylor J, Smith EJ, Davison W, Sugiyama M. Resolving and modeling the effects of Fe and Mn redox cycling on trace metal behavior in a seasonally anoxic lake. Geochimica et Cosmochimica Acta. **2005**, 69(8), 1947-60.
[21] Rozan TF, Taillefert M, Trouwborst RE, Glazer BT, Ma S, Herszage J, et al. Iron-sulfur-phosphorus cycling in the sediments of a shallow coastal bay: Implications for sediment nutrient release and benthic macroalgal blooms. Limnology and Oceanography. **2002**, 47(5), 1346-54.
[22] Abell JM, Özkundakci D, Hamilton DP, Miller SD. Relationships between land use and nitrogen and phosphorus in New Zealand lakes. Marine and Freshwater Research. **2011**, 62(2), 162-75.
[23] Abell JM, Hamilton DP. Bioavailability of phosphorus transported during storm flow to a eutrophic, polymictic lake. New Zealand Journal of Marine and Freshwater Research. **2013**, 47(4), 481-9.
[24] Burger DF, Hamilton DP, Pilditch CA. Modelling the relative importance of internal and external nutrient loads on water column nutrient concentrations and phytoplankton biomass in a shallow polymictic lake. Ecological Modelling. **2008**, 211(3-4), 411-23.

[25] Molot LA, Watson SB, Creed IF, Trick CG, McCabe SK, Verschoor MJ, et al. A novel model for cyanobacteria bloom formation: The critical role of anoxia and ferrous iron. Freshwater Biology. **2014**, 59(6), 1323-40.
[26] Pearson LK, Hendy CH, Hamilton DP, Silvester WB. Nitrogen-15 Isotope Enrichment in Benthic Boundary Layer Gases of a Stratified Eutrophic Iron and Manganese Rich Lake. Aquatic Geochemistry. **2012**, 18(1), 1-19.
[27] Gao Y, Cornwell JC, Stoecker DK, Owens MS. Effects of cyanobacterial-driven pH increases on sediment nutrient fluxes and coupled nitrification-denitrification in a shallow fresh water estuary. Biogeosciences. **2012**, 9(7), 2697-710.
[28] Abell JM, Özkundakci D, Hamilton DP. Nitrogen and Phosphorus Limitation of Phytoplankton Growth in New Zealand Lakes: Implications for Eutrophication Control. Ecosystems. **2010**, 13(7), 966-77.
[29] Hamilton DP, O'Brien KR, Burford MA, Brookes JD, McBride CG. Vertical distributions of chlorophyll in deep, warm monomictic lakes. Aquatic Sciences. **2010**, 72(3), 295-307.
[30] Pearson LK. 2012, University of Waikato, Hamilton.
[31] Lowe DJ, Shane PAR, Alloway BV, Newnham RM. Fingerprints and age models for widespread New Zealand tephra marker beds erupted since 30,000 years ago: a framework for NZ-INTIMATE. Quaternary Science Reviews. **2008**, 27(1-2), 95-126.
[32] Forsyth DJ. Distribution and production of Chironomus in eutrophic Lake Ngapouri. New Zealand Journal of Marine & Freshwater Research. **1986**, 20(1), 47-54.
[33] Hartland A, Fairchild IJ, Lead JR, Baker A. Fluorescent properties of organic carbon in cave dripwaters: Effects of filtration, temperature and pH. Science of the Total Environment. **2010**, 408(23), 5940-50.
[34] (APHA) APHA, Association) AAWW, Federation WE. *Standard Methods for the Examination of Water & Wastewater* 2012 (American Water Works Assn).
[35] Parkhurst DLA, C.A.J. User's guide to PHREEQC (Version 2) – a computer program for speciation, reaction-path, 1D-transport, and inverse geochemical calculations. USGS Water Resour Inv Rep. **1999**, 99–4259.
[36] Dzombak DA, Morel FMM. *Surface Complexation Modeling: Hydrous Ferric Oxide* 1990 (Wiley-Interscience: New York).
[37] Tonkin JW, Balistrieri LS, Murray JW. Modeling sorption of divalent metal cations on hydrous manganese oxide using the diffuse double layer model. Applied Geochemistry. **2004**, 19(1), 29-53.
[38] Karamalidis AK, Dzombak DA. *Surface Complexation Modeling: Gibbsite* 2010.
[39] Sholkovitz ER, Copland D. The chemistry of suspended matter in Esthwaite Water, a biologically productive lake with seasonally anoxic hypolimnion. Geochimica et Cosmochimica Acta. **1982**, 46(3), 393-410.
[40] Hamilton-Taylor J, Davison W. in *Physics and Chemistry of Lakes* Eds. Lerman A, Imboden D, Gat J)1995, pp. 217-63 (Springer Berlin Heidelberg).
[41] Jakobsen R, Postma D. Redox zoning, rates of sulfate reduction and interactions with Fe-reduction and methanogenesis in a shallow sandy aquifer, Romo, Denmark. Geochimica et Cosmochimica Acta. **1999**, 63(1), 137-51.
[42] Gustafsson JP, Lumsdon DG, Simonsson M. Aluminium solubility characteristics of spodic B horizons containing imogolite type materials. Clay Minerals. **1998**, 33(1), 77-86.
[43] Gustafsson JP, Bhattacharya P, Karltun E. Mineralogy of poorly crystalline aluminium phases in the B horizon of Podzols in southern Sweden. Applied Geochemistry. **1999**, 14(6), 707-18.
[44] Postma D, Jessen S, Hue NTM, Duc MT, Koch CB, Viet PH, et al. Mobilization of arsenic and iron from Red River floodplain sediments, Vietnam. Geochimica et Cosmochimica Acta. **2010**, 74(12), 3367-81.
[45] Dixit S, Hering JG. Comparison of Arsenic(V) and Arsenic(III) Sorption onto Iron Oxide Minerals: Implications for Arsenic Mobility. Environmental Science & Technology. **2003**, 37(18), 4182-9.

598 [46] Cui Y, Weng L. Arsenate and phosphate adsorption in relation to oxides composition in soils:
599 LCD modeling. Environmental Science and Technology. **2013**, 47(13), 7269-76.
600 [47] Ghosh A, Chakrabarti S, Ghosh UC. Fixed-bed column performance of Mn-incorporated
601 iron(III) oxide nanoparticle agglomerates on As(III) removal from the spiked groundwater in lab
602 bench scale. Chemical Engineering Journal. **2014**, 248, 18-26.
603 [48] Puccia V, Luengo C, Avena M. Phosphate desorption kinetics from goethite as induced by
604 arsenate. Colloids and Surfaces A: Physicochemical and Engineering Aspects. **2009**, 348(1-3), 221-7.
605 [49] Hartland A, Lead JR, Slaveykova VI, O'Carroll D, Valsami-Jones E. The Environmental
606 Significance of Natural Nanoparticles. Nature Education Knowledge. **2013**, 4(8), 7.
607 [50] Parks GA. The isoelectric points of solid oxides, solid hydroxides, and aqueous hydroxo
608 complex systems. Chemical Reviews. **1965**, 65(2), 177-98.
609 [51] Su C, Harsh JB, Bertsch PM. Sodium and chloride sorption by imogolite and allophanes. Clays
610 & Clay Minerals. **1992**, 40(3), 280-6.

611

612

613

614

615

616

617

618 **Table 1** Major ion concentration and charge balance data for profile 1 of Lake Ngapouri, March 2014

	Cations mg L^{-1}									Anions mg L^{-1}						
Depth (m)	pH	Na	K	Ca	Mg	Fe	Mn	Al	NH_4	Cl	HCO_3	SO_4	NO_3	NO_2	PO_4	CB %
0.0	6.4	8.4	4.6	7.8	2.0	0.0	0.0	0.0	0.0	7.0	25.7	24.6	0.02	0.0	< 0.01	-4.0
0.5	6.3	8.8	4.6	8.2	2.0	0.1	0.0	0.0	0.0	6.9	24.4	24.4	0.03	0.0	< 0.01	-1.1
1.0	6.4	8.6	4.6	8.0	2.0	0.1	0.0	0.0	0.0	6.9	24.7	24.4	0.01	0.0	< 0.01	-2.2
1.5	6.4	9.0	4.7	8.2	2.1	0.0	0.0	0.0	0.0	7.0	26.3	24.5	0.01	0.0	< 0.01	-1.9
2.0	6.4	8.6	4.4	8.1	2.0	0.0	0.0	0.0	0.0	6.9	26.8	24.5	0.01	0.0	< 0.01	-3.8
2.5	6.4	8.9	4.3	8.1	2.1	0.0	0.0	0.0	0.0	6.9	24.8	24.5	0.01	0.0	< 0.01	-1.8
3.0	6.4	8.7	4.4	8.2	2.1	0.0	0.0	0.0	0.0	7.0	25.7	24.7	0.01	0.0	< 0.01	-2.7
3.5	6.5	8.8	4.3	8.0	2.0	0.0	0.0	0.0	0.0	6.9	24.9	24.5	0.01	0.0	< 0.01	-2.2
4.0	6.4	8.6	4.3	8.0	2.0	0.0	0.0	0.0	0.0	6.9	24.3	24.5	0.01	0.0	< 0.01	-2.4
4.5	7.4	8.8	4.6	8.2	2.1	0.1	0.0	0.0	0.0	7.0	23.4	24.7	0.02	0.0	< 0.01	-0.5
5.0	6.4	8.8	4.5	9.4	2.0	0.0	0.0	0.0	0.0	7.0	33.6	24.7	0.03	0.0	< 0.01	-5.2
5.5	6.5	9.2	4.4	8.5	2.1	0.0	0.0	0.0	0.0	7.0	25.6	24.6	0.02	0.0	< 0.01	-0.4
6.0	6.5	8.7	4.5	8.2	2.1	0.0	0.0	0.0	0.0	7.1	24.9	25.0	0.01	0.0	< 0.01	-2.4
6.5	5.9	8.8	4.4	8.1	2.0	0.0	0.0	0.0	0.0	7.0	25.4	24.8	0.01	0.0	< 0.01	-2.7
7.0	6.8	8.6	4.5	7.8	1.9	0.1	0.0	0.0	0.1	7.0	25.0	24.5	0.01	0.0	165.8	-51.9
7.5	6.5	9.2	9.4	8.2	2.1	0.1	0.0	0.0	0.0	6.9	25.7	24.0	0.02	0.0	15.0	-1.8
8.0	6.5	9.1	4.0	7.9	2.0	0.0	0.0	0.0	0.0	7.1	24.8	24.7	0.01	0.0	< 0.01	-2.8
8.5	6.5	8.8	4.2	8.1	2.0	0.0	0.0	0.0	0.0	7.0	26.1	23.9	0.02	0.0	< 0.01	-2.5
9.0	6.4	9.0	4.3	8.1	2.1	0.0	0.1	0.0	0.0	7.0	28.8	23.0	0.01	0.0	< 0.01	-2.5
9.5	6.7	9.0	4.2	8.0	2.0	0.0	0.1	0.0	0.0	7.2	30.1	22.7	0.01	0.0	< 0.01	-4.4
10.0	6.8	9.6	12.5	8.6	2.1	0.0	0.2	0.0	0.0	7.0	32.8	23.1	0.04	0.0	24.5	-4.5
10.5	6.7	9.2	5.6	8.3	2.1	0.0	0.1	0.0	0.0	7.0	33.3	21.7	0.01	0.0	3.6	-4.1
11.0	6.7	9.4	4.6	8.4	2.0	0.0	0.3	0.0	0.0	7.2	33.8	22.1	0.02	0.0	1.0	-4.2

11.5	6.6	9.8	4.8	8.5	2.0	0.1	0.6	0.0	0.1	7.1	34.3	21.8	0.01	0.0	1.1	-2.3
12.0	6.5	9.4	4.4	8.5	2.1	0.2	0.7	0.0	0.1	7.0	38.5	21.4	0.01	0.0	0.4	-5.0
12.5	6.4	9.9	4.5	8.7	2.1	0.7	0.6	0.0	0.4	7.0	37.5	20.8	0.01	0.0	0.1	-0.9
13.0	6.5	9.8	4.4	8.6	2.1	0.6	0.6	0.0	0.3	7.0	41.1	21.2	0.01	0.0	< 0.01	-4.3
13.5	6.6	10.0	4.4	8.5	2.1	1.3	0.6	0.0	0.5	7.0	39.3	20.8	0.01	0.0	< 0.01	-1.6
14.0	6.5	9.5	4.4	8.5	2.0	1.7	0.6	0.0	0.6	7.0	39.0	20.3	0.01	0.0	< 0.01	-1.2
14.5	6.7	9.8	4.3	8.6	2.1	1.5	0.6	0.0	0.5	7.1	39.5	21.0	0.01	0.0	< 0.01	-1.6
15.0	6.5	9.6	4.2	8.3	2.1	1.4	0.6	0.0	0.6	7.1	37.6	20.9	0.01	0.0	< 0.01	-1.5
15.5	6.5	9.9	4.3	8.5	2.2	2.0	0.6	0.0	0.6	7.1	43.9	20.2	0.01	0.0	< 0.01	-2.6
16.0	6.5	9.6	4.2	8.2	2.0	2.1	0.6	0.0	0.6	7.2	40.1	20.5	0.01	0.0	< 0.01	-2.1
16.5	6.5	10.0	4.3	8.3	2.2	2.5	0.6	0.0	0.7	7.2	42.0	20.3	0.01	0.0	< 0.01	-1.2
17.0	6.5	10.3	4.3	8.4	2.3	2.5	0.6	0.0	0.6	7.2	40.5	20.6	0.01	0.0	< 0.01	0.7
17.5	6.6	10.3	4.3	8.6	2.2	2.8	0.6	0.0	0.8	7.3	42.8	20.0	0.02	0.0	< 0.01	0.3
18.0	6.6	9.9	4.3	8.4	2.2	3.3	0.7	0.0	0.8	7.2	43.3	18.8	0.01	0.0	< 0.01	1.2
18.5	6.5	9.5	4.1	8.1	2.1	2.9	0.6	0.0	0.7	7.2	42.2	19.6	0.02	0.0	< 0.01	-1.5
19.0	6.5	10.1	4.2	8.5	2.2	3.3	0.7	0.0	0.8	7.3	42.4	19.3	0.01	0.0	< 0.01	1.5
19.5	6.5	9.5	4.0	8.2	2.1	3.1	0.7	0.0	0.9	7.3	43.1	19.0	0.00	0.0	< 0.01	-0.9
20.0	6.6	9.7	4.1	8.3	2.0	2.5	0.6	0.0	0.7	7.3	40.2	20.2	0.01	0.0	< 0.01	-0.8
20.5	6.5	9.7	4.0	8.3	2.1	2.4	0.5	0.0	0.7	7.4	38.8	21.0	0.00	0.0	< 0.01	-0.8
21.0	6.7	9.8	4.1	8.5	2.1	3.5	0.7	0.0	1.0	7.3	43.6	18.8	0.01	0.0	< 0.01	1.0
21.5	6.5	9.2	3.9	8.4	2.2	0.0	0.0	0.0	0.0	7.8	25.1	27.2	0.01	0.0	< 0.01	-4.3
22.0	6.5	9.6	4.0	8.1	2.1	3.5	0.7	0.0	0.9	7.3	45.9	18.4	0.01	0.0	< 0.01	-1.6
22.5	6.6	10.4	4.1	8.8	2.2	3.9	0.7	0.0	1.0	7.4	45.4	18.9	0.01	0.0	< 0.01	1.7

CB% = percentage charge balance.

Table 2 Major ion concentration and charge balance data for profile 2 of Lake Ngapouri, March 2014

	Cations mg L^{-1}									Anions mg L^{-1}						
Depth (m)	pH	Na	K	Ca	Mg	Fe	Mn	Al	NH_4	Cl	HCO_3	SO_4	NO_3	NO_2	PO_4	CB%
0.0	6.3	9.4	6.7	7.7	1.9	0.1	0.0	0.0	0.1	7.6	25.6	24.9	0.08	0.01	<0.01	-31.23
0.5	6.8	8.7	7.2	8.1	2.0	0.1	0.0	0.0	0.0	7.2	22.0	24.8	0.02	0.01	<0.01	-0.76
1.0	6.9	8.5	6.1	8.0	2.0	0.1	0.0	0.0	0.0	7.3	24.0	24.9	0.08	0.01	<0.01	-3.17
1.5	6.6	9.7	4.4	8.4	2.1	0.1	0.0	0.0	0.0	7.2	23.6	24.6	0.02	0.01	<0.01	0.77
2.0	6.5	10.0	3.7	8.3	2.1	0.1	0.0	0.0	0.0	7.2	24.7	24.7	0.04	0.01	<0.01	-0.05
2.5	7.1	8.6	4.7	8.1	2.0	0.1	0.0	0.0	0.0	7.4	30.9	25.3	0.00	0.01	<0.01	-7.66
3.0	6.3	8.9	4.4	7.9	2.1	0.1	0.0	0.0	0.0	7.3	19.0	24.9	0.00	0.01	<0.01	1.32
3.5	5.6	8.2	4.7	7.8	2.0	0.1	0.0	0.0	0.0	7.4	22.2	25.4	0.00	0.01	<0.01	-3.09
4.0	5.0	8.5	4.8	8.2	2.0	0.1	0.0	0.0	0.0	7.4	22.8	25.5	0.00	0.02	<0.01	-2.07
4.5	5.6	8.3	4.4	7.8	1.9	0.1	0.0	0.0	0.0	7.4	23.0	25.1	0.01	0.00	<0.01	-3.94
5.0	5.3	8.9	4.8	8.5	2.1	0.1	0.0	0.0	0.0	7.4	36.4	25.3	0.03	0.00	<0.01	-9.15
5.5	5.5	8.6	4.7	8.2	2.1	0.1	0.0	0.0	0.0	7.5	24.2	25.2	0.02	0.00	<0.01	-2.38
6.0	5.6	8.2	4.5	8.0	1.9	0.1	0.0	0.0	0.0	7.4	24.3	25.4	0.00	0.02	<0.01	-4.56
6.5	5.4	8.2	4.7	8.1	2.0	0.1	0.0	0.0	0.0	7.5	21.9	25.6	0.00	0.03	<0.01	-2.31
7.0	5.7	8.5	4.8	8.3	2.1	0.1	0.0	0.0	0.0	7.4	24.5	25.5	0.02	0.00	<0.01	-2.50
7.5	4.8	8.8	4.9	8.5	2.2	0.1	0.0	0.0	0.0	7.5	20.5	26.3	0.00	0.01	<0.01	1.08
8.0	5.6	8.4	4.7	8.2	2.0	0.1	0.0	0.0	0.0	7.5	20.4	25.7	0.00	0.02	<0.01	-0.62
8.5	5.8	8.3	4.7	8.2	2.1	0.1	0.0	0.0	0.0	7.5	23.4	25.6	0.00	0.02	<0.01	-2.85
9.0	5.5	8.3	4.7	8.3	2.0	0.1	0.1	0.0	0.0	7.4	26.4	24.8	0.00	0.01	<0.01	-4.06
9.5	5.9	8.5	4.8	8.3	2.1	0.1	0.0	0.0	0.0	7.5	23.9	25.3	0.01	0.00	<0.01	-2.14
10.0	5.5	8.8	4.7	8.3	2.0	0.1	0.0	0.0	0.0	7.2	24.8	22.9	0.00	0.01	<0.01	0.24
10.5	5.6	8.5	4.6	8.2	2.0	0.0	0.1	0.0	0.0	7.2	29.3	22.5	0.01	0.00	<0.01	-3.92

11.0	5.5	8.6	4.7	8.4	2.0	0.1	0.7	0.0	0.0	7.1	34.4	21.4	0.00	0.02	<0.01	-4.14
11.5	5.7	8.9	4.7	8.6	2.1	0.2	0.6	0.0	0.2	7.2	26.4	21.6	0.00	0.02	<0.01	3.01
12.0	6.4	9.1	4.5	7.9	2.1	0.2	0.5	0.0	0.1	7.3	31.9	22.1	0.00	0.03	<0.01	-3.26
12.5	6.4	9.1	4.5	7.9	2.0	0.2	0.5	0.0	0.2	7.3	32.9	21.7	0.00	0.03	<0.01	-3.88
13.0	6.4	9.4	4.6	7.9	2.1	0.7	0.6	0.0	0.5	7.3	35.2	21.1	0.02	0.01	<0.01	-2.26
13.5	6.7	8.8	4.4	7.7	2.0	0.4	0.5	0.0	0.3	7.4	34.0	22.2	0.01	0.01	<0.01	-5.63
14.0	6.5	8.8	4.8	7.9	2.1	0.8	0.3	0.0	0.3	7.4	31.2	22.9	0.02	0.01	<0.01	-2.78
14.5	6.5	9.4	5.0	8.4	2.1	1.6	0.6	0.0	0.6	7.3	40.9	20.2	0.02	0.01	<0.01	-1.81
15.0	6.6	9.1	5.1	8.3	2.2	0.3	0.2	0.0	0.1	7.5	31.2	24.5	0.02	0.01	<0.01	-3.87
15.5	6.5	8.6	4.4	7.6	2.0	1.3	0.6	0.0	0.7	7.2	41.1	19.8	0.02	0.01	<0.01	-6.42
16.0	6.4	9.2	4.6	8.1	2.1	1.3	0.5	0.0	0.5	7.3	37.2	21.1	0.01	0.01	<0.01	-2.53
16.5	6.5	9.5	5.0	8.7	2.2	1.6	0.6	0.0	0.6	7.3	33.4	20.7	0.01	0.01	<0.01	3.57
17.0	6.4	9.4	4.9	8.2	2.1	2.7	0.6	0.0	0.8	7.3	42.5	19.5	0.01	0.01	<0.01	-1.05
17.5	6.5	9.0	4.9	8.2	2.0	2.6	0.6	0.0	0.8	7.3	36.5	19.6	0.02	0.01	<0.01	1.78
18.0	6.6	9.0	4.9	8.4	2.1	1.5	0.4	0.0	0.5	7.4	33.3	22.0	0.01	0.01	<0.01	-0.28
18.5	6.5	9.5	5.0	8.6	2.2	3.4	0.7	0.0	0.8	7.3	40.5	18.7	0.01	0.01	<0.01	3.32
19.0	6.5	9.5	5.0	8.2	2.1	3.2	0.7	0.0	0.9	7.2	40.6	18.4	0.01	0.02	<0.01	2.56
19.5	6.6	9.3	5.1	8.6	2.2	1.7	0.4	0.0	0.5	7.5	36.1	22.2	0.01	0.01	<0.01	-0.50
20.0	6.6	9.4	5.1	8.5	2.2	3.1	0.6	0.0	0.7	7.4	37.7	20.3	0.01	0.01	<0.01	3.11
20.5	6.6	9.2	4.8	8.1	2.1	1.8	0.6	0.0	0.7	3.6	36.2	10.4	0.01	0.01	<0.01	15.16
21.0	6.5	9.3	4.8	8.4	2.1	1.7	0.6	0.0	0.6	4.2	37.0	11.8	0.01	0.01	<0.01	12.57

CB% = percentage charge balance.

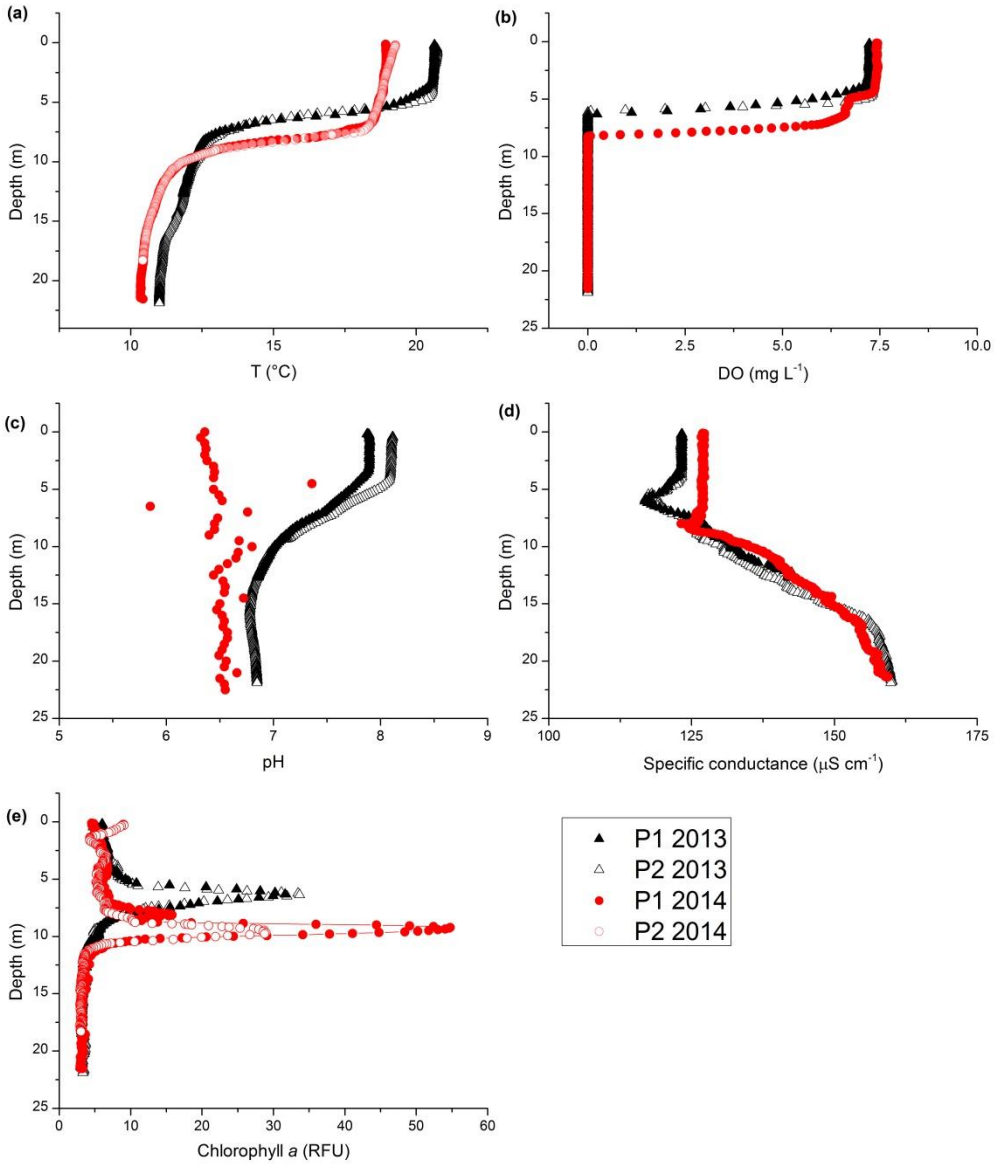

628

629 **Figure 1** Physiochemical gradients within Lake Ngapouri in March 2013 and 2014 recorded using a
630 conductance-temperature-dissolved oxygen probe. Due to a faulty CTD pH probe in 2014, the pH
631 data presented in (c) were determined using a bench-top pH meter. RFU = relative fluorescence units.

632

633

634

635

636

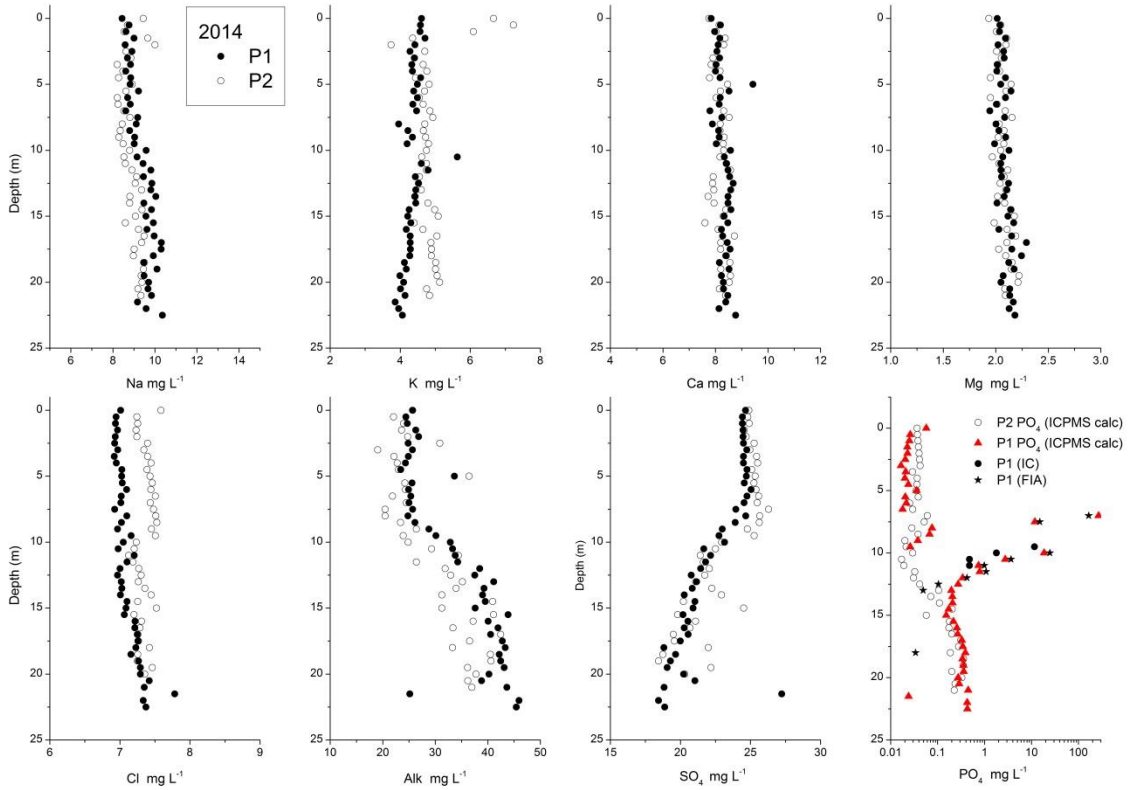

Figure 2 Depth profiles of major ion chemistry in Lake Ngapouri measured in samples taken in March 2014. Phosphate (PO_4) data are shown from two direct analyses [ion chromatography (IC), flow injection analysis (FIA)] and one indirect prediction [inductively coupled plasma mass spectrometry (ICPMS)]. The elemental P data from ICPMS were used to estimate the equivalent concentration of phosphate to test whether the ICPMS results predominantly reflected the presence of orthophosphate species and to provide a maximum possible phosphate concentration in the lake waters.

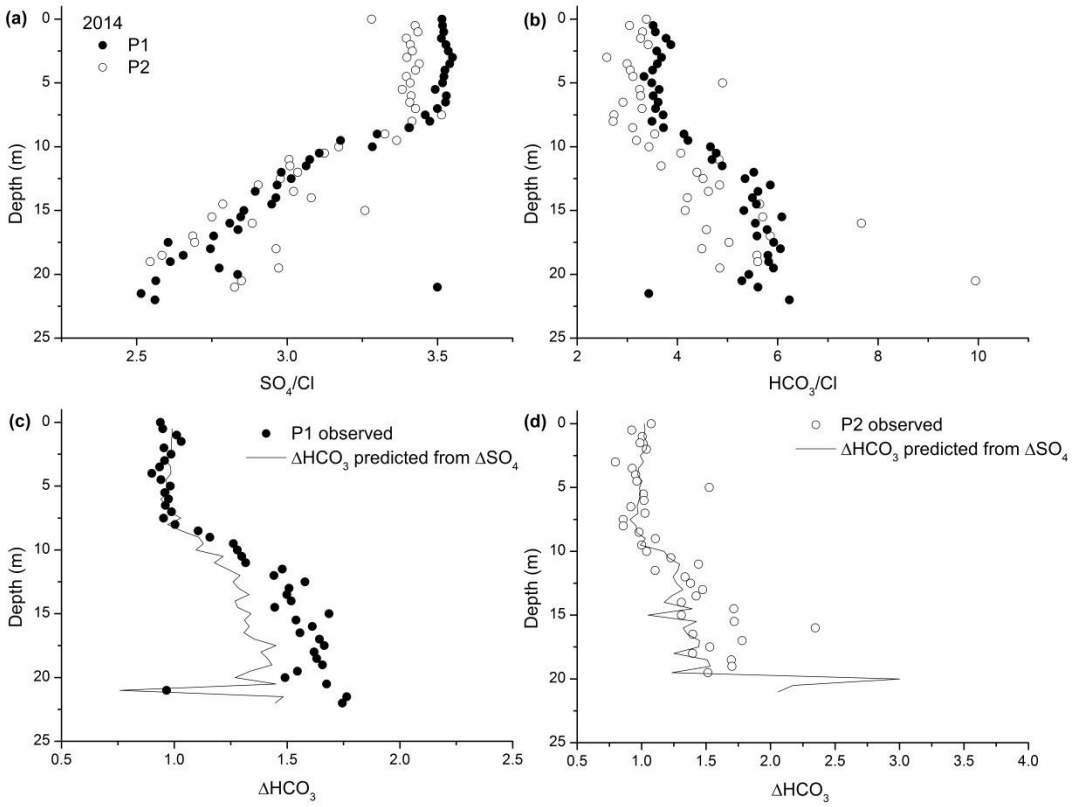

Figure 3 Change in sulfate (SO_4) concentration and bicarbonate alkalinity concentration (HCO_3) in profiles 1 and 2 from 2014. In a and b, the sulfate and bicarbonate concentrations are shown normalised to chloride (Cl) to provide a measure of the change due to biogeochemical rather than hydrodynamic factors. In c and d, the observed change in bicarbonate with depth (ΔHCO_3) is plotted with the predicted ΔHCO_3 calculated from the observed change in sulfate concentration (ΔSO_4) with respect to the sulfate concentration in the upper 10 m.

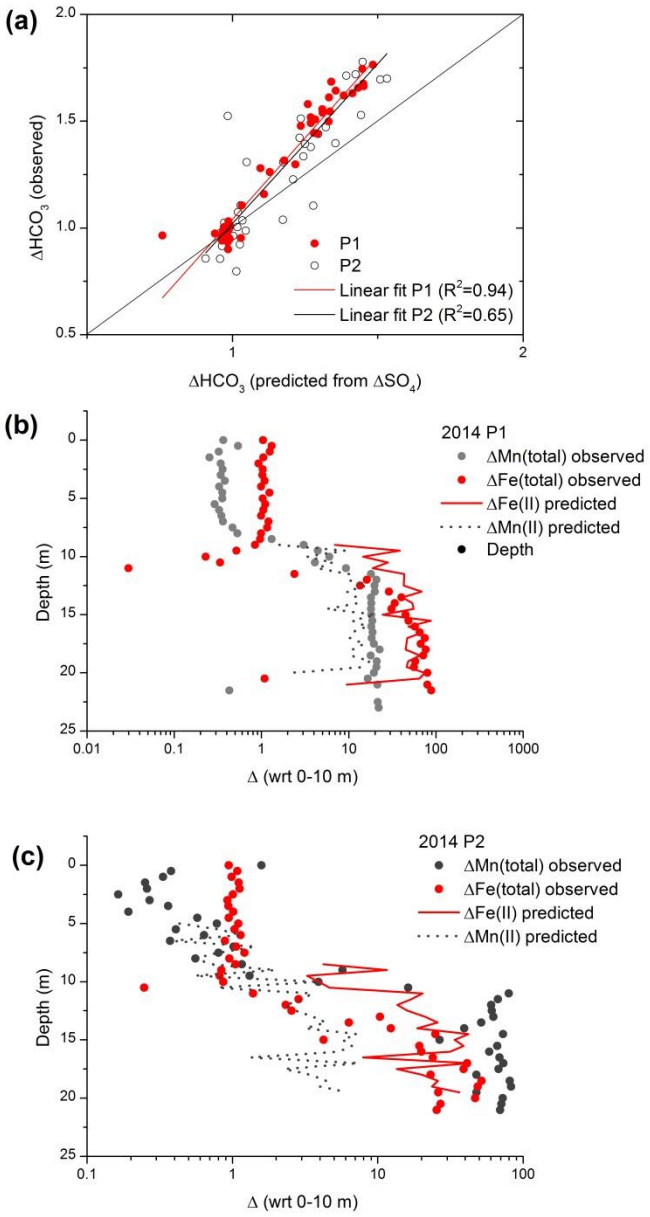

Figure 4 Reconciling the discrepancy between the predicted change in alkalinity in Lake Ngapouri based on changes in sulfate (a) to the observed changes in iron (Fe) and manganese (Mn) concentration in profile 1 (b) and 2 (c) with respect to (wrt) 0-10m depth. See text for description of calculations.

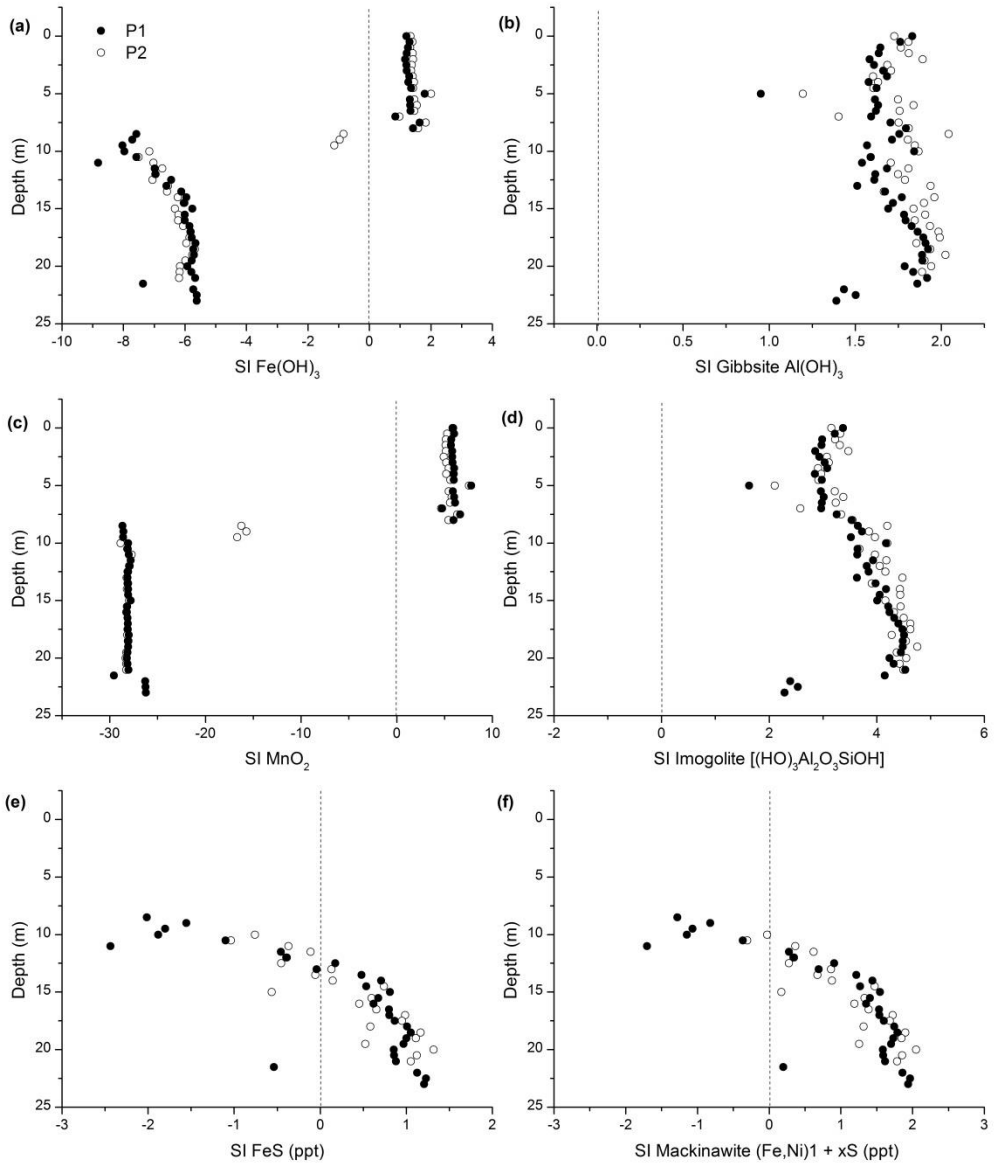

Figure 5 Calculated saturation indices (SIs) for (a) iron, (b) aluminium and (c) manganese hydroxides, the paracrystalline imogolite (d) and (e) iron monosulfides and (f) iron-nickel sulfides, in Lake Ngapouri waters corresponding to profile 1 (P1) and profile 2 (P2) from the 2014 field campaign. Vertical dashed lines denote SI = 0.

691

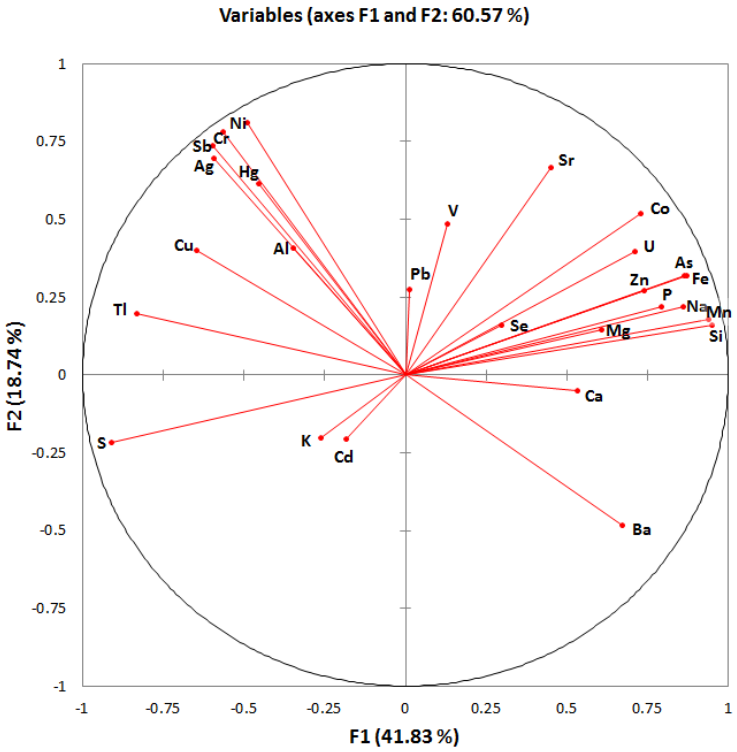

692

693 **Figure 6** Principal components analysis of the 2014 trace element dataset from Lake Ngapouri (n=90).

694

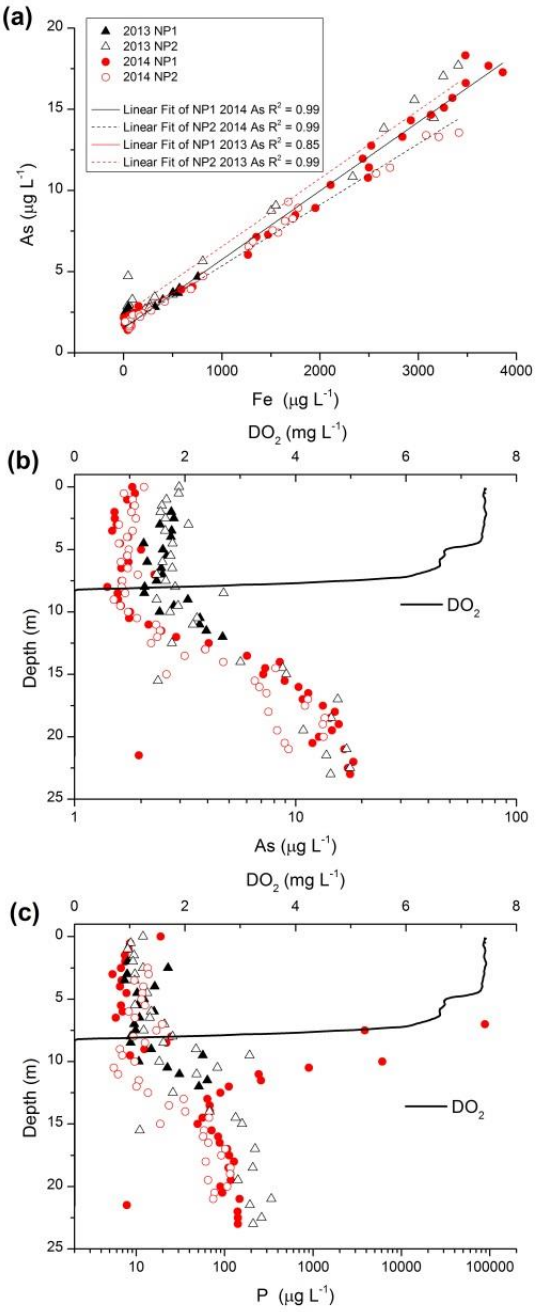

695

696 **Figure 7** Overprint of redox zonation on the trace elements arsenic (As) and phosphorus (P) in Lake
697 Ngapouri in March 2013 and 2014. (a) Strong linear correlation between iron (Fe) and arsenic (As). (b)
698 Depth profiles of As and (c) P from both years.

699

700

701

702

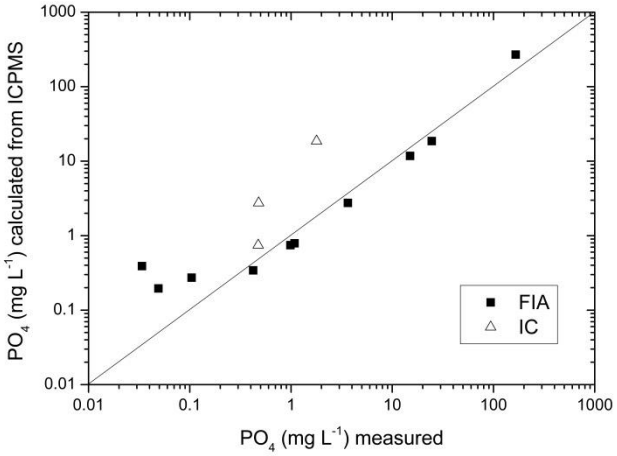

703

704 **Figure 8** Comparison of phosphate (PO_4) analysed by flow injection analysis (FIA) and ion
705 chromatography (IC) with the calculated phosphate concentration from elemental P measured by
706 inductively coupled plasma mass spectrometry (ICPMS). This demonstrates that the concentrations
707 measured by FIA and ICPMS are concordant but that at low elemental P concentrations, estimates
708 based on ICPMS measurements are likely to over-predict the actual phosphate concentration. In
709 epilimnetic waters phosphate was generally below detection by FIA at < 0.01 mg L^{-1} phosphate
710 (equivalent to < 0.004 mg L^{-1} P-PO_4). This implies that P in the epilimnion and deeper hypolimnetic
711 waters was predominantly present as other P-bearing species, such as dissolved organic compounds.

712

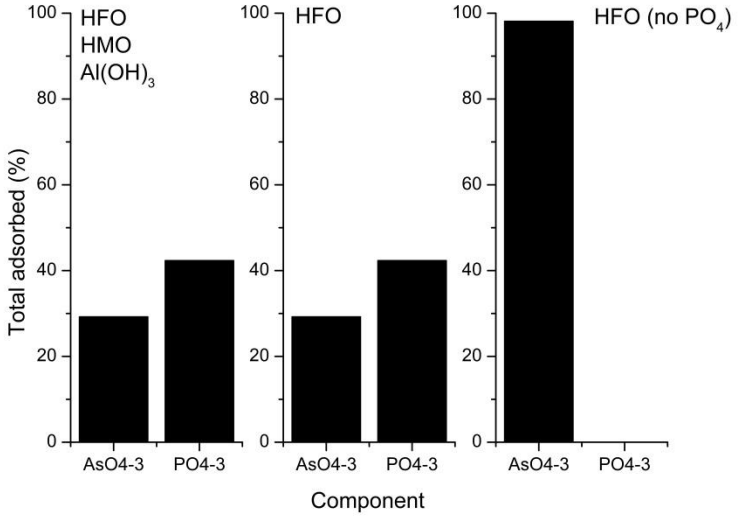

713

714 **Figure 9** Results of surface complexation modelling of phosphate (PO_4^{3-}/HPO_4^{2-}/$H_2PO_4^-$) and arsenate
715 (AsO_4^{3-}/$HAsO_4^{2-}$/ $H_2AsO_4^-$) species adsorption to hydrous manganese oxides (HMO), hydrous ferric
716 oxides (HFO) and aluminium hydroxides (gibbsite) in the geochemical code VMINTEQ 3.0.
717 Conditions of pH and major ion chemistry were set to the average from 0 to 10 m depth in Ngapouri
718 from March 2014.

719